



Fermi National Accelerator Laboratory

FERMILAB-Pub-78/35-EXP
7120.381

(Submitted to Sov. J. Nucl. Phys.)

THE REAL PART OF THE P-P AND P-D FORWARD SCATTERING AMPLITUDES FROM 50 TO 400 GeV

E. Jenkins

University of Arizona, Tucson, Arizona 85721 USA

and

A. Kuznetsov, B. Morozov, V. Nikitin, P. Nomokonov,
Y. Pilipenko, A. Sandacz, and V. Smirnov
Joint Institute for Nuclear Research, Dubna, USSR

and

E. Malamud and R. Yamada
Fermi National Accelerator Laboratory
Batavia, Illinois 60510 USA

and

D. Gross
University of Rochester, Rochester, New York 14627 USA

April 1978

THE REAL PART OF THE P-P AND P-D
FORWARD SCATTERING AMPLITUDES FROM 50 TO 400 GEV^{*}

E. Jenkins
University of Arizona, Tucson, Arizona 85721 USA

and

A. Kuznetsov, B. Morozov, V. Nikitin, P. Nomokonov,
Y. Pilipenko, A. Sandacz,[†] and V. Smirnov
Joint Institute for Nuclear Research, Dubna, USSR

and

E. Malamud and R. Yamada
Fermi National Accelerator Laboratory
Batavia, Illinois 60510 USA

and

D. Gross[§]
University of Rochester, Rochester, New York 14627 USA

April 1978

^{*}This work supported in part by the U. S. Department of Energy, the U. S. National Science Foundation, and the USSR State Committee for Atomic Energy.

[†]Present Address: Institute of Nuclear Research, Warsaw, Poland.

[§]Present Address: Fermi National Accelerator Laboratory, Batavia, Illinois 60510 USA.

ABSTRACT

Proton-proton and proton-deuteron elastic scattering has been measured for incident proton laboratory energy from 50 to 400 GeV. Both reactions were investigated by detection of the recoil particles. The minimum $|t|$ value in the p-p data was 0.0005 (GeV/c)^2 and 0.0008 (GeV/c)^2 for the p-d data; values which lie within the Coulomb region. From these experiments we have determined the ratios of the real part to imaginary part of the forward scattering amplitude, ρ_{pp} and ρ_{pd} , for p-p and p-d scattering. We find that ρ_{pp} and ρ_{pd} show systematic differences that are explicable in terms of a model which assumes $\rho_{pp} = \rho_{pn}$. Using a Glauber approach and a sum of exponentials for the deuteron form factor we obtain ρ_{pn} for p-n scattering.

I. INTRODUCTION

Previous experiments at the Fermi National Accelerator Laboratory have yielded measurements of the ratio of the real part to imaginary part of the forward scattering amplitude, ρ_{pp} , for pp elastic scattering^{1,2} as well as the slope of the forward diffraction peak, b , of p-p³ and p-d elastic scattering.⁴ Recent measurements have been reported from the ISR at CERN on ρ_{pp} and the resultant dispersion relation implications on σ_{pp} at ultra high energies.⁵ Additional measurements at Serpukhov on p-d elastic scattering below 70 GeV have yielded a parameterization of the deuteron form factor $|S(t)|$, and the ratio of the real part to imaginary part ρ_{pd} , for p-d scattering.^{6,7} Further analysis using a Glauber approach has resulted in values reported from the Serpukhov data from the ratio of the real part to imaginary part ρ_{pn} , for p-n scattering.⁸

We have extended these measurements to higher energies and with lower momentum transfer, $|t|$, further into the Coulomb and Coulomb-nuclear interference regions. It is observed that ρ_{pp} rises and crosses through zero at approximately 335 GeV, a consequence and reflection of the rise in the total cross section. Isotopic spin invariance in strong interactions makes the prediction that asymptotically at high energies we would expect to find $\rho_{pp} = \rho_{pn}$. Our motivation was to test this prediction at high energies and in a single experimental setup.

In Section II we describe the experiment and details of the analysis. In Section III we tabulate our p-p data at 52,

80, 199, 261, 303 and 398 GeV and our p-d data at 49, 82, 182, 281, 379 and 397 GeV. In Section IV we discuss the results of the fits and obtain values for the real part of the forward scattering amplitude for p-p and p-d scattering. In this section the deuteron is considered a single target particle. We discuss the energy dependence of ρ_{pp} and ρ_{pd} . In Section V we use the Glauber approach to fit ρ_{pn} . In Section VI we summarize our conclusions.

II. EXPERIMENTAL PROCEDURE AND APPARATUS

Figure 1 is a schematic layout of the experiment. The circulating beam in the main ring of the Fermilab accelerator intercepted a low density gas jet target of hydrogen or deuterium. Recoil particles were detected at a distance of 7.5 meters by sets of solid state silicon detectors. The detectors, detector box, and ion guide were under vacuum and mounted on a movable assembly; the angle could be varied remotely. The detector, jet profile size, and 7.5 meters distance determine an angular resolution of ± 0.8 mrad, a factor of 3 improvement over previous experiments.¹⁻⁴

The $|t|$ values studied were $0.0005 < |t| < 0.03 \text{ (GeV/c)}^2$ for hydrogen, corresponding to recoil angles $11 < \omega < 90$ mrad and ranges in silicon $2 < R < 1600 \text{ } \mu\text{m}$. The $|t|$ values for deuterium were $0.0008 < |t| < 0.08 \text{ (GeV/c)}^2$ corresponding to recoil angles $8 < \omega < 75$ mrad and ranges in silicon $3 < R < 1500 \text{ } \mu\text{m}$.

The typical jet operating parameters were density $2 \times 10^{-8} \text{ g/cm}^3$, jet width (RMS) $\pm 6 \text{ mm}$, and jet pulse length 100 msec. At this density and at $|t| = .0006 \text{ (GeV/c)}^2 \text{ (pp)}$ or $|t| = .001 \text{ (GeV/c)}^2 \text{ (pd)}$ the correction to $d\sigma/dt$ due to multiple scattering of the outgoing recoil particle was about 3%. The Fermilab main circulating beam had typical operating parameters: intensity 1.8×10^{13} protons/pulse, beam size 2 mm diameter. Data runs were taken simultaneously at different energy points along the magnetic ramp rise in the range $50 \text{ GeV} < E_{\text{lab}} < 400 \text{ GeV}$. During the pp runs 3 jets/pulse were used; the pd data was obtained using 4 jets/pulse. The magnetic field in the accelerator was recorded every 30 msec, or every .4 GeV in the incident beam energy.

The recoil protons or deuterons were detected by sandwiches of two solid-state detectors. The detectors used were totally depleted surface barrier silicon with typical dimensions $4 \times 20 \text{ mm}^2$. The front detectors ranged from 15 μm to 250 μm thick and the back detectors from 200 μm to 1500 μm . The recoil particle usually stopped in the back detector. For the lowest $|t|$ range the particle range was less than the thickness of the front detector. The detectors were movable remotely and set at varying angles during the experiment. Two stacks of detectors were permanently fixed and were used to monitor the jet-beam interaction rate.

A schematic diagram of the electronics is shown in Fig. 2. Pulses from the detectors were fed to preamplifiers and then

to amplifiers. The amplified ΔE signal from a given front detector was discriminated and used to trigger a commercial CAMAC peak sensing ADC. During readout of a stack the inputs to all other stacks were inhibited. Thus all channels had the same percentage dead time ($\leq 3\%$).

The ADC's for the front and back detectors were each supplemented with a TDC which measured the time difference between the front and back detector signals. The scanner scanned the ADC and TDC outputs, and these outputs plus stack identification bits were stored as two CAMAC words in one of two fast 64 word buffer memory units. When one buffer memory unit was full it was disabled and read into a PDP-11 computer. During this time the other buffer memory unit was enabled and data collection continued without interruption. After storage on a magnetic disk, events were written onto a magnetic tape for permanent storage. In addition, the computer generated the gates and timing for the experiment, event histograms, stack display patterns, beam spill histograms, and calibration tasks. Typical data rates were 1,000 events per jet pulse distributed over 8 detector stacks.

The linearity of the electronics was checked by sending test pulses into test inputs of the preamps and recording the output pulse heights. The ADC integral linearity was 0.2%. The differential linearity was 1.5%.

III. DATA ANALYSIS AND CROSS SECTION TABLE

A. Data Analysis

The bit patterns were sorted into 256 x 256 plots of the front detector ΔE vs. the back detector $E - \Delta E$. The mass of a particle stopping in the back element is given by the empirical formula

$$m = m_p \left[\frac{\alpha}{d_F} \left[(T_F + T_B)^\beta - T_B^\beta \right] \right]^{1/(\beta-1)} \quad (1)$$

where $\alpha = 0.0133$, $\beta = 1.73$, d_F is the thickness of the front detector in mm, and $T_F(T_B)$ is the energy deposited in the front (back) detector in MeV. Using Eq. (1) we define deuterons by the cuts $1.5 < m/m_p < 2.5$ and protons by the cuts $0.5 < m/m_p < 1.5$.

The momentum distribution of the recoil is shown in Fig. 3. The momentum spectra were fitted over the range $> 5.0 \sigma$ (σ is the Gaussian standard deviation) to a formula which contained Gaussian plus exponential (background) terms. The number of elastic events was obtained after applying cuts at $\pm 4 \sigma$ and subtracting the background, which was determined from the fit. The background was ~1% except for the lowest $|t|$ deuteron data where background was ~3%. We have checked that fits made with different "smooth" background terms (linear, quadratic) give approximately the same result. Our low background is due to the long ion guide and good shielding. The width of the elastic

peak is consistent with a total angular resolution of ± 0.8 mrad expected from our jet size (± 6 mm) and detector geometry (± 4 mm). The good angular resolution led to a negligible ($< 0.2\%$) inelastic background under the elastic peak, arising from reactions $pp \rightarrow Xp$ or $pd \rightarrow Xd$.

The number of elastic events in each detector, ΔN , in solid angle $\Delta\Omega$, were converted to $d\sigma/dt$ as follows:

$$\frac{d\sigma}{dt} = \frac{\Delta N}{\Delta\Omega} \frac{\pi}{2m \sqrt{|t|}} \left(\frac{d\sigma}{d\Omega} \right)_{\text{fixed}} / \left(\frac{\Delta N}{\Delta\Omega} \right)_{\text{fixed}} \quad (2)$$

where $\left(\frac{d\sigma}{d\Omega} \right)_{\text{fixed}}$ and $\left(\frac{\Delta N}{\Delta\Omega} \right)_{\text{fixed}}$ are for the fixed monitors. $\frac{\Delta N}{\Delta\Omega}$ and $\left(\frac{\Delta N}{\Delta\Omega} \right)_{\text{fixed}}$ are the number of elastic events after applying the geometrical and resolution corrections. At the smallest $|t|$ values our geometrical correction was about 1.5% and correction due to resolution about 7%. The correct normalization was obtained in the final fits from the optical theorem.

B. Systematic Errors

1. Angle

The absolute angle of the detector assembly was determined from the energy of the elastic peaks wholly contained in the front detectors. Detectors were calibrated with an alpha particle source, ${}_{90}\text{Th}^{234}$ (5.446, 5.684, 6.04, 6.277, 6.774, 8.786 MeV). The absolute angles determined from the elastic peaks and alpha particle energy calibrations, when compared with angle

data from survey measurements show our estimated angular uncertainty to be $\lesssim 0.15$ mrad. Recent measurements with p/d and p/He target mixtures indicate that this angle offset is independent of the particle type, range, or detector angle. Shielding reduced the magnetic field in our detector system to ≤ 0.03 gauss. This minimized angular errors at very low $|t|$. Due to our angular uncertainty the systematic error on $d\sigma/dt$ in the interference region is about 1%.

2. Area

The uncertainty in detector area is $\pm 0.15\%$.

3. Nuclear Interactions

The effect of deuteron and proton interactions in the silicon detector are approximately proportional to the particle range. For our t range the effects are $\leq 0.07\%$.

C. Cross Section Table

The cross sections for p-p at 52, 80, 199, 261, 303, 398 GeV and for p-d at 49, 82, 182, 281, 379, 397 GeV are given in Table I. The errors listed are statistical. The absolute normalizations, determined in the fits from the optical theorem point, are uncertain by $\approx 0.7\%$ for p-p and $\approx 0.5\%$ for p-d scattering. The p-p data at 398 GeV and the p-d data at 379 GeV are shown in figures 4 and 5.

IV. DETERMINATION OF ρ_{pp} AND ρ_{pd}

Our results for p-p elastic cross sections, listed in Table I, have been fitted to the Bethe interference formula⁹ which includes electromagnetic effects.

$$\frac{d\sigma}{dt} = \pi |f_n + f_c|^2 \quad (3)$$

where the nuclear and Coulomb scattering amplitudes take the forms

$$f_n = \frac{\sigma_{tot}}{4\pi k} (\rho_{pp} + i) e^{bt/2} \quad (4)$$

$$f_c = \frac{2\alpha k}{t} G_p^2(t) e^{i\alpha\beta} \quad (5)$$

The free parameters in the fit are ρ_{pp} and the overall normalization which sets a scale to the values listed in Table I. $\Delta\rho/\Delta b$ and $\Delta\rho/\Delta\sigma$ can be used to calculate the change in ρ due to a change in the assumed values of b and σ_{tot} .

In Eq. (4) we have assumed that the real and imaginary parts have the same t dependence and that spin effects may be neglected.

For σ_{tot} and b we use empirical fits to the data of Carroll et al.,¹⁰ $\sigma_{tot}(mb) = 50.866 - 5.2302 \ln S_{pp} + 0.5437 \ln S_{pp}'$, and

Bartenev et al.,³ $b(s) = 8.27 + 0.556 \ln S_{pp}$.¹¹ In Eq. (5) α

is the fine structure constant, $G_P(t) = \frac{1}{(1 + |t|/0.71)^2}$.

the proton electromagnetic form factor, and $\alpha\phi = 2\alpha\ln \frac{1.06\hbar}{R\sqrt{|t|}}$ the Coulomb phase with $R = \sqrt{10} \text{ mb}^{1/2}$.

The χ^2 minimization results for ρ_{pp} , the ratio of the real to imaginary parts of the forward scattering amplitude, are listed in Table II. Typical χ^2 's are 1.2-1.3 per degree of freedom. In Fig. 6 we show these values together with previously published results.^{5,11} Results on ρ_{pp} from the Fermilab experiment^{1,2} are not shown on Fig. 6 since too many points in the same energy region would be confusing. Our results are in agreement with the previous experiment and have somewhat smaller statistical and systematic errors. Furthermore in the present case tables of differential cross sections are given so readers may fit other models to the data. An empirical expression valid within our energy range is

$$\rho_{pp}(s) = (-0.490 \pm 0.034) + (0.076 \pm 0.006) \ln S_{pp}. \quad (6)$$

The solid curve shown in Fig. 6 is derived from a dispersion relation

$$\text{Re } A = C + \frac{E}{4\pi^2} \int_0^\infty dE' \left[\frac{\sigma_T(E')}{E' - E} - \frac{\bar{\sigma}_T(E')}{E' + E} \right] \quad (7)$$

where σ_T and $\bar{\sigma}_T$ are proton-proton and anti-proton-proton total cross sections. The normalization of the curve (adjustment of C) is arbitrary using our data and that of Amaldi et al.³ The dashed curve in Fig. 6 is calculated assuming only vacuum exchange.

Our results for p-d elastic cross sections, listed also in Table I, have been fitted with Eq. (3), the Bethe interference formula, where we treat the deuteron as a single particle. In this case the nuclear amplitude is parameterized as a sum of exponentials^{4,12}

$$f_n = \frac{\sigma_{\text{tot}}}{4\pi k} (\rho_{\text{pd}} + i) e^{bt/2} \times \left[0.34e^{\frac{141.5t}{4}} + 0.58e^{\frac{26.1t}{4}} + 0.08e^{\frac{15.5t}{4}} \right] \quad (8)$$

where we assume that $b(s) = b_{\text{pp}} = 8.27 + 0.556 \ln S_{\text{pp}}$ and use an empirical fit to the published pd total cross section^{10,13}
 $\sigma_{\text{tot,pd}}(\text{mb}) = 99.73 - 9.40 \ln S_{\text{pd}} + 0.829 \ln^2 S_{\text{pd}}$. The Coulomb amplitude is written as

$$f_c = \frac{2\alpha k}{t} G_p(t) G_d(t) e^{i\alpha\beta} \quad (9)$$

with $G_d(t) = e^{(25.95t + 60t^2)/2}$ and $\alpha\beta = 2\alpha \ln \frac{1.06k}{R\sqrt{|t|}}$ with
 $R = 2.7 \sqrt{10} \text{ mb}^{1/2}$.

In Table II we list our results for the ratio of the real to imaginary parts of the forward scattering amplitude, ρ_{pd} . An empirical expression valid in our energy range is:

$$\rho_{\text{pd}} = (-0.450 \pm 0.035) + (0.070 \pm 0.006) \ln S_{\text{pp}} \quad (10)$$

The main contribution to the systematic error in ρ_{pp} (± 0.009)

and in ρ_{pd} (± 0.008) is the angular uncertainty (0.15 mrad) in the position of the detectors.¹⁵ In Fig. 7 we show our ρ_{pd} values together with previously published results.⁶ The solid line shown is our $\rho_{pp}(s)$ parameterization, Eq. (6).

Pertinent to our understanding of the relationship between ρ_{pd} and ρ_{pp} is the following Glauber derivation. If one expresses the deuteron forward scattering amplitude as

$$f_d = f_p + f_n + i\hbar \langle r^{-2} \rangle_d f_p f_n \quad (11)$$

where we know the deuteron inverse radius squared, $\langle r^{-2} \rangle_d = I_G = 0.033 \text{ mb}^{-1}$. (I_G will be discussed in the next section.)

If we further assume that the forward proton and neutron amplitudes are equal

$$f_n = f_p = \frac{\sigma_{tot}}{4\pi\hbar} (\rho_{pp} + i) \quad (12)$$

then substitution of Eq. (12) into Eq. (11) and omission of the higher order ρ_{pp}^2 term, will give

$$f_d = \frac{\sigma_{tot}}{2\pi\hbar} \left[\rho_{pp} (1 - \delta) + i (1 - \frac{\delta}{2}) \right]. \quad (13)$$

In the above we use the notation of a Glauber screening parameter $\delta \equiv \langle r^{-2} \rangle \frac{\sigma_{tot}}{4\pi} \approx 0.111$. The implication of Eq. (13) is that we would expect

$$\rho_{pd} = \frac{\text{Re } f_d}{\text{Im } f_d} = \rho_{pp} \cdot \frac{(1 - \delta)}{(1 - \frac{\delta}{2})} = 0.941 \rho_{pp}. \quad (14)$$

This is a relationship satisfied by the data in Table II and Table III and displayed in the lines drawn on Fig. 7. Both ρ_{pp} and ρ_{pd} cross zero at 335 GeV. Equation (14) predicts that ρ_{pd} and ρ_{pp} will be zero at the same energy. Using the empirical fits to our data ($\rho = \rho_0 + \rho_1 \ln s$) as expressed by Eqs. (6) and (10) we find

$$\rho_{lpd}/\rho_{lpp} = 0.92 \pm 0.11 \quad (15)$$

in good agreement with the prediction. Since the derivation is based upon the equivalency of the proton and neutron our results support the idea of isotopic spin invariance in proton neutron collisions at high energies.

V. THE GLAUBER APPROACH AND ρ_{pn}

In the Glauber approach^{12,14-16} elastic p-d scattering is described as a coherent sum of Coulomb, single-nucleon, and double-nucleon scattering. Assuming only s-wave contribution to the form factor and only elastic rescattering we can write

$$\frac{d\sigma}{dt} = \pi \left| S(t/4) (A_C + A_p + A_n) + A_G \right|^2, \quad (16)$$

where

$$A_C = \frac{2\alpha\hbar}{t} e^{b_{pp}t/2} e^{i\eta}$$

$$A_p = e^{i\chi_{cp}} \frac{\sigma_{pp}}{4\pi\hbar} (\rho_{pp} + i) e^{b_{pp}t/2},$$

$$A_n = e^{i\chi_{cn}} \frac{\sigma_{pn}}{4\pi\hbar} (\rho_{pn} + i) e^{b_{pn}t/2},$$

$$A_G = e^{i\chi_{cpn}} \frac{i\hbar \sigma_{pp} \sigma_{pn}}{(4\pi\hbar)^2} (\rho_{pp} + i) (\rho_{pn} + i) e^{t(b_{pp} + b_{pn})/8} I_G.$$

$S(t/4)$ is the deuteron form factor, b_{pp} , b_{pn} , ρ_{pp} , ρ_{pn} and σ_{pp} , σ_{pn} are the slope parameters, real to imaginary forward nuclear scattering-amplitude ratios, and total cross sections for pp and pn scattering, respectively, and η , χ_{cp} , χ_{cn} , and χ_{cpn} are phases between the amplitudes. We assume t independence for ρ_{pp} and ρ_{pn} , as no experimental information exists on this point. I_G is the Glauber integral:

$$I_G = \frac{1}{2} \int_{-\infty}^{\infty} S(t) e^{b_{pp}t/2} e^{b_{pn}t/2} dt. \quad (17)$$

We calculate phases using the formulas in Ref. 12:

$$\chi_{cp} = 0.10, \chi_{cn} = 0.11, \chi_{cpn} = 0.10,$$

$$\eta = (2/137.03) \{ \ln[2p_{lab}/\sqrt{t}] - 0.577$$

For the p-p total cross section we refer to the empirical formula given previously. We assume that $\sigma_{pn} = \sigma_{pp}$. For b_{pn}

$= b_{pp}$ we take the empirical fit,³ $b_{pp} = 8.27 + 0.556 \ln S_{pp}$. For ρ_{pp} we use our measured values summarized in the empirical fit, Eq. (6). The spherical deuteron form factor, $S_0(t/4)$, is given by a sum of exponentials

$$S(t/4) = S_0(t/4) = A_1 e^{B_1 t/4} + A_2 e^{B_2 t/4} + (1 - A_1 - A_2) e^{B_3 t/4} \quad (18)$$

with the coefficients previously given in Eq. (8). Calculations show that inclusion of a quadrupole form factor is significant only at large $|t|$ values and introduces a maximum contribution of $\approx 1.6\%$ at our highest $|t|$.

The results of the Glauber analysis are given in Table III and shown in Figs. 8 and 9. The free parameters are ρ_{pn} and I_G . One notes a larger statistical error on ρ_{pn} in comparison with the ρ_{pd} statistical error. This is inherent in the analysis. Not shown in Fig. 8 are the systematic errors in our ρ_{pn} values introduced by uncertainty in the deuteron form factor $S(t/4)$. These systematic errors are of the order of our statistical errors. In Fig. 8 is shown the total error corridor on our ρ_{pp} results for comparison of the ρ_{pn} values with ρ_{pp} . The shadow correction is shown in Fig. 9. We have also tried other hypotheses for b_{pn} , e.g. using the empirical fit found in Ref. 4, $b_{pn} = 5.57 \pm 1.15 \ln S_{pp}$. Using this shrinkage instead of the more reasonable $b_{pn} = b_{pp}$ shifts the ρ_{pn} values up by about one standard deviation.

In (16) we neglected the Coulomb amplitude contribution to the double scattering term. This problem was considered by Franco and Varma.¹² For pd elastic scattering in the Serpukhov energy range they estimated that the difference between the Glauber formula which includes all double scattering terms and the more approximate Eq. (16) is less than 2% for $d\sigma/dt$ in the Coulomb-nuclear interference region. The difference in the value of ρ_{pn} obtained from the two formulas is ~ 0.03 . Another complication is that in our energy range inelastic intermediate states may contribute to the double scattering term. It is not expected that inelastic and elastic contributions have the same t -dependence.

To investigate how the problems mentioned above may affect our result on ρ_{pn} we also determined ρ_{pn} by another method using the Glauber formula for the pd elastic scattering forward amplitude. Using (11) and the optical theorem one can derive the following:

$$\begin{aligned} \rho_{pn} = \frac{1}{\sigma_{pn}} \{ & (\sigma_{pd}\rho_{pd} - \sigma_{pp}\rho_{pp}) (1 + \frac{\langle r^{-2} \rangle_d}{4\pi} \sigma_{pp}) \\ & + (\sigma_{pd} - \sigma_{pp}) \frac{\langle r^{-2} \rangle_d}{4\pi} \sigma_{pp}\rho_{pp} \} \end{aligned} \quad (19)$$

To estimate ρ_{pn} we used ρ_{pd} given in Table II and parameterized σ_{pp} , σ_{pd} and ρ_{pp} as described in Section IV. We assume $\sigma_{pn} = \sigma_{pp}$ and values for $\langle r^{-2} \rangle_d = I_G$ were taken from Table III. The systematic error in ρ_{pn} due to the uncertainty in the double

scattering term is energy dependent and small compared to the statistical errors. If we assign an error of -20% to I_G then the resulting systematic error in ρ_{pn} is $< .005$. Comparison of ρ_{pn} obtained from (16) (Table III) with those obtained from (19) (Table IV) show no significant difference between the two methods.

VI. CONCLUSIONS

Comparison of our pp data with dispersion relation calculations show good agreement. By comparing our pp data with the prediction obtained from a simple vacuum exchange model we can estimate the importance of other exchanges (Fig. 6). ρ_{pp} and ρ_{pd} both cross zero at about 335 GeV. In Section V we showed that using a Glauber approach to obtain ρ_{pn} we found no significant difference between ρ_{pp} and ρ_{pn} . The shadow correction increases with energy (Fig. 9) but remains small, $\leq 0.03 \text{ mb}^{-1}$.

ACKNOWLEDGMENTS

We acknowledge the strong support of the Fermilab Internal Target Group under the leadership of Dr. T. Nash. V. Smelyanski helped in the target development and installation. We are grateful to Dr. Victor Matveev for useful discussions. The Dubna members of the collaboration wish to especially acknowledge the support and hospitality of the Fermilab Directorate during their stay.

REFERENCES

- ¹V. D. Bartenev et al., Phys. Rev. Lett. 31, 1367 (1973).
- ²V. D. Bartenev et al., Yad. Fiz. 23, 759 (1976); [Sov. J. Nucl. Phys. 23, 400 (1976)].
- ³V. D. Bartenev et al., Phys. Rev. Lett. 31, 1088 (1973).
- ⁴Y. Akinov, et al., Phys. Rev. D 12, 3399 (1975).
- ⁵U. Amaldi et al., Phys. Lett. 66B, (1977).
- ⁶V. D. Bartenev et al., Yad. Fiz. 15, 1174 (1972); [Sov. J. Nucl. Phys. 15, 650 (1972)]; G. G. Beznogikh, Nucl. Phys. B54, 97 (1973).
- ⁷L. S. Zolin et al., Yad. Fiz. 18, 55 (1973); [Sov. J. Nucl. Phys. 18, 30 (1974)].
- ⁸G. G. Beznogikh et al., Yad. Fiz. 18, 348 (1973); [Sov. J. Nucl. Phys. 18, 179 (1974)].
- ⁹H. Bethe, Ann. Phys. (N.Y.) 3, 190 (1958).
- ¹⁰A. S. Carroll et al., Phys. Rev. Lett. 33, 928 (1974).
- ¹¹ S_{pp} and S_{pd} are expressed in units of 1 GeV^2 .
- ¹²V. Franco and G. K. Varma, Phys. Rev. D 12, 225 (1975).
- ¹³Yu. P. Gorin et al., Yad. Fiz. 17, 309 (1973); [Sov. J. Nucl. Phys. 17, 157 (1973)].
- ¹⁴R. J. Glauber, Phys. Rev. 100, 242 (1955).
- ¹⁵The 49 and 397 GeV data have somewhat larger systematic errors than the other 4 pd energies. If they are omitted from

the fit then $\rho_{pd} = (-0.473 \pm .052) + (0.073 \pm 0.007) \ln S_{pp}$.

¹⁶V. Franco and R. J. Glauber, Phys. Rev. 142, 1195 (1966).

V. Franco and E. Coleman, Phys. Rev. Lett. 17, 827 (1966).

¹⁷G. G. Beznogikh et al., Phys. Lett. 39B, 411 (1972).

TABLE 1. Differential Cross Sections $d\sigma/dt$ for p-p and p-d.

-t [(GeV/c) ²]			-t [(GeV/c) ²]			
dσ/dt [mb/(GeV/c) ²]			dσ/dt [mb/(GeV/c) ²]			
(dσ/dt)			(dσ/dt)			
pp → pp 52 GeV	0.00063	765.90	17.34	0.00077	756.23	21.98
	0.00065	724.49	16.61	0.00100	596.68	14.61
	0.00076	553.59	7.54	0.00150	395.00	8.97
	0.00100	366.71	5.50	0.00178	341.63	13.20
	0.00124	263.87	5.41	0.00184	334.00	17.17
	0.00131	257.86	7.28	0.00212	360.62	12.88
	0.00132	244.52	3.99	0.00219	313.55	12.26
	0.00133	248.51	7.11	0.00235	311.44	5.60
	0.00159	203.57	5.66	0.00243	320.19	5.68
	0.00161	191.74	5.44	0.00268	299.16	4.58
	0.00162	191.11	3.39	0.00284	289.46	8.86
	0.00193	161.20	3.82	0.00291	293.72	8.88
	0.00205	152.86	2.38	0.00304	286.02	4.31
	0.00214	149.05	3.25	0.00357	281.07	7.68
	0.00223	150.19	5.25	0.00407	258.64	7.54
	0.00225	143.14	5.12	0.00412	253.59	4.42
	0.00242	129.94	2.66	0.00415	259.15	7.55
	0.00248	136.74	3.88	0.00438	254.69	6.40
	0.00249	134.87	2.78	0.00456	249.00	3.67
	0.00280	117.62	2.58	0.00502	243.61	5.79
0.00302	115.44	2.80	0.00510	239.98	4.32	
0.00339	101.05	3.19	0.00588	223.14	3.68	
0.00342	101.73	3.19	0.00671	219.15	3.81	
0.00344	108.44	2.47	0.00749	197.37	5.83	
0.00383	98.71	3.14	0.00929	206.45	8.39	
0.00386	102.74	3.21	0.01070	178.40	3.26	
0.00409	94.06	2.07	0.01152	176.33	5.28	
0.00435	102.48	2.72	0.01227	174.95	6.29	
0.00457	92.73	1.90	0.01402	156.46	3.49	
0.00466	94.36	1.98	0.01484	136.61	7.13	
0.00483	89.36	3.09	0.01500	150.11	7.64	
0.00486	90.75	3.12	0.01529	150.54	3.13	
0.00518	88.12	1.90	0.01563	146.17	3.38	
0.00561	90.78	2.15	0.01662	139.45	2.77	
0.00593	83.83	1.91	0.01766	138.27	4.00	
0.00633	87.52	2.00	0.01943	126.05	2.66	
0.00647	82.55	2.88	0.02056	125.10	4.12	
0.00651	85.63	1.96	0.02126	116.61	2.03	
0.00652	84.86	2.93	0.02264	106.90	3.11	
0.00708	81.54	2.23	0.02383	107.58	2.30	
0.00713	82.76	2.25	0.02490	102.38	3.89	
0.00739	80.21	1.61	0.02511	102.29	3.91	
0.00780	82.02	2.01	0.02610	99.90	1.77	
0.00803	77.13	1.58	0.02851	87.41	3.34	
0.00842	77.00	2.59	0.02874	91.93	3.32	
0.00889	78.85	1.48	0.02914	86.07	1.88	
0.00944	77.95	2.25	0.02961	84.86	1.67	
0.00946	77.32	1.69	0.03096	83.26	2.00	
0.00986	77.61	1.93	0.03304	75.81	1.59	
0.01033	77.87	1.75	0.03477	69.44	1.59	
0.01057	74.22	2.26	0.03623	71.12	1.61	
0.01061	75.22	1.51	0.03628	73.56	2.96	
0.01171	74.24	1.65	0.03653	73.40	3.03	
0.01218	73.68	1.78	0.03902	62.88	1.37	
0.01253	70.54	1.28	0.04137	55.51	1.32	
0.01340	73.47	1.56	0.04192	58.53	1.47	
0.01424	68.36	1.49	0.04197	61.04	2.34	
0.01474	70.66	1.58	0.04225	57.41	2.33	
0.01530	70.41	1.47	0.04744	48.33	1.08	
0.01555	69.13	1.33	0.04803	46.73	1.16	
0.01565	68.91	1.65	0.04808	50.45	2.19	
0.01700	68.05	1.38	0.05392	37.77	0.96	
0.01754	63.63	1.45	0.05456	36.91	0.89	
0.01797	64.95	1.40	0.05482	36.01	1.31	
0.02000	62.77	1.28	0.05487	36.86	1.30	
0.02068	65.33	1.41	0.06151	31.12	0.83	
0.02175	63.97	1.47				
0.02334	60.02	1.19				
0.02514	58.32	1.00				
0.02753	57.49	1.22				
0.02877	58.32	1.25				
0.03060	55.21	1.07				

	0.00066	672.58	13.61
	0.00067	655.77	13.43
	0.00080	494.86	8.50
	0.00104	344.26	6.46
	0.00135	223.31	5.53
	0.00137	222.65	3.51
	0.00164	177.93	4.62
pp → pp	0.00166	184.49	4.72
	0.00168	173.73	3.89
80 GeV	0.00200	144.74	3.05
	0.00211	138.91	2.72
	0.00220	137.74	2.60
Normalization	0.00231	130.45	2.67
uncertainty	0.00250	124.13	2.58
	0.00288	110.12	2.13
0.69%	0.00311	105.17	2.22
	0.00348	101.52	2.59
	0.00351	99.61	2.56
	0.00353	97.61	2.06
	0.00392	96.98	2.22
	0.00395	95.84	2.20
	0.00419	89.58	1.69
	0.00446	89.42	1.44
	0.00468	88.13	1.64
	0.00478	86.57	1.55
	0.00495	88.47	2.42
	0.00498	88.69	2.42
	0.00575	83.00	1.20
	0.00648	80.75	1.52
	0.00663	81.45	2.16
	0.00666	80.61	1.38
	0.00667	80.76	2.15
	0.00724	76.19	1.84
	0.00729	76.80	1.84
	0.00755	76.16	1.29
	0.00797	77.09	1.54
	0.00966	72.01	1.29
	0.01007	72.47	1.42
	0.01083	72.07	1.28
	0.01197	70.67	1.24
	0.01243	70.58	1.45
	0.01279	67.51	1.09
	0.01294	71.37	1.41
	0.01452	67.81	1.26
	0.01503	68.37	1.44
	0.01594	63.07	1.30
	0.01732	64.81	1.24
	0.01788	65.23	1.29
	0.01831	64.74	1.18
	0.01858	63.08	1.18
	0.01960	63.72	1.16
	0.02038	61.29	1.10
	0.02106	60.18	1.15
	0.02215	59.32	1.16
	0.02377	58.02	1.01
	0.02559	58.74	1.14
	0.02802	56.46	1.04
	0.02928	56.34	1.43

	0.00092	632.28	13.34
	0.00103	549.71	12.75
	0.00106	528.00	12.34
	0.00155	402.41	9.58
	0.00159	400.19	9.46
	0.00207	332.66	5.11
	0.00233	318.22	5.44
pd → pd	0.00244	312.87	5.71
	0.00255	309.11	4.94
82 GeV	0.00256	306.69	5.46
	0.00261	308.89	5.47
	0.00272	309.04	5.12
Normalization	0.00354	277.05	4.59
uncertainty	0.00375	262.49	5.13
	0.00382	263.09	5.14
0.47%	0.00394	253.62	4.13
	0.00430	241.01	4.42
	0.00445	247.89	4.83
	0.00460	238.91	4.09
	0.00483	236.41	4.24
	0.00533	240.42	5.66
	0.00590	221.88	3.96
	0.00653	215.14	3.10
	0.00691	209.24	4.53
	0.00699	210.84	3.39
	0.00700	210.94	4.56
	0.00718	209.39	3.62
	0.00737	201.09	3.06
	0.00766	201.05	3.20
	0.00775	209.04	2.76
	0.00858	199.06	3.26
	0.00899	192.28	3.05
	0.00967	185.44	3.89
	0.00974	185.35	2.71
	0.00977	182.99	3.85
	0.01067	172.35	2.67
	0.01125	175.61	2.11
	0.01188	168.33	4.64
	0.01199	171.87	4.70
	0.01208	168.79	3.01
	0.01363	154.66	2.05
	0.01403	154.10	2.33
	0.01445	150.73	2.76
	0.01454	148.29	2.48
	0.01458	148.25	2.73
	0.01638	138.83	2.26
	0.01667	137.69	2.73
	0.01713	137.48	2.48
	0.01727	137.25	2.48
	0.01843	127.24	2.11
	0.01923	124.01	1.90
	0.01970	123.88	1.67
	0.02134	121.02	2.66
	0.02145	112.81	2.47
	0.02148	116.94	2.60
	0.02366	103.69	1.59
	0.02457	100.60	1.97
	0.02473	101.70	1.98
	0.02706	90.98	1.83
	0.02763	95.69	1.56
	0.02835	88.48	1.31
	0.03129	82.09	1.17
	0.03193	78.34	1.85
	0.03211	78.48	1.85
	0.03369	75.40	1.36
	0.03476	71.00	0.98
	0.03758	63.78	1.60
	0.03773	65.05	1.03
	0.03778	64.67	1.62
	0.03954	63.31	1.07
	0.04066	57.93	0.99
	0.04347	52.59	1.39
	0.04368	53.96	1.41
	0.04509	50.35	0.75
	0.04581	51.40	0.91
	0.04674	47.21	0.91
	0.05355	37.85	0.78
	0.05489	36.83	0.66
	0.05921	31.88	0.60
	0.06054	30.03	0.66
	0.06226	29.21	0.56
	0.06655	25.35	0.57
	0.06797	24.49	0.54
	0.06978	22.08	0.46
	0.07583	18.81	0.50

	0.00066	689.53	15.50
	0.00068	648.06	14.79
	0.00080	477.58	6.36
	0.00104	319.27	4.77
	0.00129	231.56	4.69
	0.00136	216.36	6.30
	0.00137	210.40	3.45
pp + pp	0.00138	215.02	6.28
	0.00165	164.55	4.76
199 GeV	0.00167	165.29	4.76
	0.00169	165.03	2.99
	0.00201	139.63	3.34
Normalization	0.00212	132.94	2.06
uncertainty	0.00222	130.00	2.81
	0.00231	127.61	4.51
0.56%	0.00233	119.68	4.34
	0.00251	116.06	1.94
	0.00258	118.37	2.39
	0.00290	106.40	2.31
	0.00313	107.35	2.56
	0.00350	92.76	2.93
	0.00353	92.59	2.92
	0.00356	94.06	2.14
	0.00396	98.73	3.04
	0.00422	88.99	1.90
	0.00450	86.65	2.28
	0.00472	84.33	1.67
	0.00482	83.96	1.73
	0.00499	87.60	2.99
	0.00503	81.23	2.87
	0.00535	84.84	1.77
	0.00580	78.41	1.80
	0.00613	79.47	1.76
	0.00654	81.71	1.83
	0.00669	81.21	2.76
	0.00672	77.66	1.24
	0.00673	77.08	2.67
	0.00731	81.00	2.18
	0.00736	79.36	2.15
	0.00762	76.64	1.47
	0.00805	77.77	1.88
	0.00847	77.07	1.74
	0.00869	74.95	2.46
	0.00917	76.53	1.39
	0.00975	73.19	1.56
	0.01018	73.78	1.79
	0.01066	71.94	1.58
	0.01095	73.38	1.43
	0.01209	70.52	1.52
	0.01256	69.33	1.63
	0.01292	69.48	1.21
	0.01309	71.33	1.43
	0.01381	68.03	1.38
	0.01467	63.73	1.35
	0.01519	67.73	1.46
	0.01578	67.30	1.38
	0.01602	63.66	1.16
	0.01613	65.73	1.56
	0.01751	64.53	1.24
	0.01808	63.15	1.41
	0.01851	63.76	1.34
	0.02060	60.71	1.21
	0.02130	62.84	1.31
	0.02241	59.55	1.33
	0.02403	59.94	1.13
	0.02509	56.54	0.92
	0.02836	54.61	1.10
	0.02964	55.47	1.15
	0.03150	52.63	0.98

	0.00106	506.26	11.59
	0.00109	489.49	11.38
	0.00159	364.84	8.74
	0.00164	360.47	8.53
	0.00212	311.80	4.63
	0.00239	299.09	5.03
	0.00251	239.75	5.17
pd + pd	0.00262	294.49	4.63
	0.00263	295.11	5.09
182 GeV	0.00269	293.77	5.06
	0.00280	287.06	4.68
	0.00364	264.40	4.27
Normalization	0.00386	249.10	4.77
uncertainty	0.00392	241.63	4.68
	0.00405	245.73	3.86
0.33%	0.00442	240.36	4.27
	0.00457	236.12	4.47
	0.00473	237.53	3.96
	0.00496	227.19	3.98
	0.00514	236.07	2.78
	0.00547	227.94	5.32
	0.00606	222.84	3.81
	0.00671	208.02	2.88
	0.00710	208.59	4.39
	0.00718	203.53	3.20
	0.00719	202.77	4.31
	0.00738	200.57	3.35
	0.00757	204.18	3.01
	0.00787	191.43	2.98
	0.00796	199.77	2.51
	0.00881	191.76	3.09
	0.00924	184.82	2.84
	0.00993	180.14	3.72
	0.01000	182.36	2.55
	0.01003	178.32	3.69
	0.01095	171.64	2.57
	0.01156	168.42	1.92
	0.01220	166.41	4.46
	0.01231	167.26	4.47
	0.01241	163.40	2.84
	0.01400	152.55	1.94
	0.01440	150.90	2.24
	0.01484	148.38	2.67
	0.01493	149.32	2.41
	0.01497	150.86	2.69
	0.01682	135.47	2.15
	0.01712	132.72	2.58
	0.01759	132.38	2.35
	0.01773	132.72	2.35
	0.01893	125.25	2.03
	0.01974	119.60	1.78
	0.02022	122.59	1.59
	0.02190	111.11	2.43
	0.02202	110.62	2.36
	0.02206	113.08	2.46
	0.02342	106.64	1.39
	0.02430	98.78	1.50
	0.02522	96.50	1.84
	0.02539	94.60	1.82
	0.02778	89.06	1.74
	0.02836	91.25	1.46
	0.02910	84.37	1.22
	0.03171	77.10	1.03
	0.03212	76.88	1.07
	0.03277	72.37	1.73
	0.03296	74.10	1.76
	0.03459	70.71	1.26
	0.03568	66.71	0.89
	0.03858	61.90	1.54
	0.03873	60.43	0.94
	0.04174	53.97	0.91
	0.04462	50.88	1.34
	0.04484	50.86	1.35
	0.04620	45.93	0.67
	0.04702	45.74	0.81
	0.04798	44.15	0.85
	0.05496	35.08	0.72
	0.05634	32.39	0.59
	0.06077	29.75	0.56
	0.06214	27.74	0.61
	0.06390	26.25	0.50
	0.06976	21.73	0.48
	0.07163	19.61	0.41
	0.07783	16.88	0.44

	0.00050	1068.32	22.69
	0.00067	639.20	14.15
	0.00069	614.66	13.82
	0.00081	463.77	8.51
	0.00106	292.73	6.01
	0.00131	226.33	4.45
	0.00138	218.49	5.99
pp + pp	0.00139	205.22	4.65
	0.00140	195.77	5.61
261 GeV	0.00167	170.85	4.91
	0.00169	164.33	4.79
	0.00171	156.63	3.84
Normalization	0.00203	136.31	3.18
uncertainty	0.00215	131.15	2.81
	0.00224	126.84	2.62
0.57%	0.00233	125.13	2.78
	0.00235	118.05	2.69
	0.00253	112.21	2.52
	0.00261	115.89	2.37
	0.00292	103.05	2.17
	0.00316	101.05	2.33
	0.00343	94.17	1.47
	0.00353	97.86	2.76
	0.00356	96.85	2.74
	0.00359	94.88	2.17
	0.00399	91.73	2.34
	0.00402	95.63	2.39
	0.00425	88.20	1.79
	0.00454	86.88	1.45
	0.00475	85.24	1.70
	0.00487	86.59	1.62
	0.00503	84.11	2.58
	0.00507	86.18	2.62
	0.00584	80.88	1.19
	0.00617	80.81	1.63
	0.00659	81.33	1.63
	0.00674	77.13	2.26
	0.00677	81.17	1.46
	0.00679	76.68	2.25
	0.00736	75.33	2.00
	0.00741	77.40	2.04
	0.00767	75.52	1.34
	0.00810	75.16	1.63
	0.00924	75.66	1.33
	0.00981	73.90	1.40
	0.01024	72.09	1.50
	0.01215	70.13	1.28
	0.01263	71.17	1.58
	0.01299	67.66	1.14
	0.01475	67.74	1.35
	0.01586	69.03	1.38
	0.01622	64.91	1.44
	0.01760	65.35	1.36
	0.01818	63.44	1.37
	0.01860	61.80	1.23
	0.01889	65.14	1.24
	0.01994	65.30	1.28
	0.02070	62.04	1.20
	0.02142	61.68	1.27
	0.02252	61.09	1.30
	0.02414	60.04	1.10
	0.02603	58.18	1.23
	0.02978	55.42	1.57

	0.00110	495.83	13.36
	0.00160	358.86	9.77
	0.00165	352.58	9.67
	0.00214	325.55	5.70
	0.00241	298.78	5.89
	0.00252	294.45	6.18
	0.00264	302.38	5.51
pd + pd	0.00265	290.07	5.84
	0.00270	291.93	5.84
281 GeV	0.00282	290.72	5.64
	0.00366	269.21	5.06
	0.00383	253.11	5.47
Normalization	0.00395	245.89	5.38
uncertainty	0.00408	246.45	4.58
	0.00445	249.12	5.12
0.38%	0.00460	245.09	5.42
	0.00476	239.57	4.63
	0.00500	240.47	4.92
	0.00517	237.71	3.32
	0.00551	226.12	6.05
	0.00610	217.09	4.37
	0.00675	214.27	3.53
	0.00685	213.29	3.24
	0.00715	208.44	5.01
	0.00723	206.86	3.83
	0.00724	205.17	4.96
	0.00743	208.64	4.11
	0.00763	206.30	3.56
	0.00793	206.54	3.78
	0.00801	198.92	2.96
	0.00887	192.80	3.59
	0.00930	189.98	3.41
	0.01000	180.30	4.31
	0.01007	176.98	2.89
	0.01010	179.84	4.29
	0.01103	171.76	3.00
	0.01164	171.93	2.33
	0.01228	173.82	5.36
	0.01240	163.14	5.13
	0.01250	161.50	3.24
	0.01409	148.70	2.21
	0.01450	148.70	2.61
	0.01494	145.88	3.05
	0.01504	145.89	2.74
	0.01507	151.33	3.12
	0.01694	134.92	2.49
	0.01724	142.31	3.23
	0.01771	134.14	2.76
	0.01785	134.57	2.75
	0.01906	124.33	2.37
	0.01938	118.68	2.06
	0.02037	123.16	1.89
	0.02206	108.24	2.71
	0.02217	113.18	2.83
	0.02221	107.31	2.69
	0.02447	102.12	1.82
	0.02557	94.42	2.11
	0.02798	91.62	2.11
	0.02856	88.13	1.63
	0.02931	87.21	1.48
	0.03194	78.40	1.24
	0.03235	77.71	1.27
	0.03300	79.04	2.17
	0.03319	79.71	2.18
	0.03483	67.97	1.39
	0.03594	67.19	1.07
	0.03885	61.86	1.80
	0.03901	59.37	1.09
	0.04087	58.13	1.16
	0.04203	52.49	1.01
	0.04494	47.16	1.44
	0.04516	49.56	1.49
	0.04661	45.02	0.77
	0.04735	46.74	0.98
	0.04832	44.18	1.01
	0.05535	35.33	0.84
	0.05675	33.53	0.71
	0.06120	29.83	0.66
	0.06258	26.87	0.67
	0.06436	25.61	0.58
	0.06879	21.31	0.57
	0.07026	21.07	0.55
	0.07839	15.94	0.49

	0.00066	670.91	13.86
	0.00067	649.69	13.54
	0.00080	463.69	5.69
	0.00104	312.73	4.29
	0.00130	229.53	4.25
	0.00137	204.41	5.59
	0.00138	207.95	3.13
pp + pp	0.00165	167.59	4.45
303 GeV	0.00166	167.99	4.45
	0.00169	163.20	2.71
	0.00201	142.50	3.10
	0.00213	129.16	1.85
Normalization	0.00223	127.82	2.56
uncertainty	0.00231	123.06	4.11
0.50%	0.00232	118.86	4.04
	0.00252	116.13	1.77
	0.00259	120.52	2.24
	0.00290	106.01	2.10
	0.00314	103.67	2.30
	0.00351	99.96	2.82
	0.00352	96.68	2.76
	0.00357	96.36	2.01
	0.00397	93.15	2.67
	0.00398	91.52	2.64
	0.00423	88.20	1.74
	0.00473	86.38	1.53
	0.00483	86.98	1.64
	0.00500	87.04	2.72
	0.00501	87.62	2.73
	0.00537	85.03	1.61
	0.00581	82.26	1.74
	0.00611	80.59	1.64
	0.00656	82.69	1.70
	0.00671	80.48	2.52
	0.00672	81.99	2.56
	0.00674	80.46	1.64
	0.00733	78.06	1.94
	0.00735	79.55	1.96
	0.00764	76.59	1.36
	0.00804	77.25	1.72
	0.00850	80.62	1.66
	0.00868	75.77	2.27
	0.00920	77.66	1.29
	0.00973	76.36	1.95
	0.00978	74.16	1.45
	0.01021	75.83	1.70
	0.01069	74.25	1.50
	0.01098	76.38	1.35
	0.01212	70.15	1.39
	0.01260	70.30	1.52
	0.01296	69.84	1.11
	0.01313	71.44	1.30
	0.01385	69.00	1.27
	0.01471	66.75	1.29
	0.01524	67.80	1.32
	0.01607	65.58	1.09
	0.01618	64.82	1.41
	0.01756	64.55	1.13
	0.01813	64.46	1.32
	0.01857	63.04	1.21
	0.02066	60.94	1.12
	0.02137	61.62	1.17
	0.02248	61.71	1.28
	0.02597	58.69	0.87
	0.02845	57.12	1.05
	0.03160	56.96	0.96

	0.00107	489.67	12.82
	0.00110	436.35	11.87
	0.00161	365.91	9.64
	0.00165	362.10	9.55
	0.00214	317.62	5.25
	0.00241	305.67	5.71
	0.00253	283.63	5.61
pd + pd	0.00264	290.78	4.94
	0.00265	289.50	5.58
379 GeV	0.00271	291.25	5.58
	0.00282	297.01	5.36
	0.00389	256.09	5.42
Normalization	0.00396	253.99	5.35
uncertainty	0.00408	255.56	4.42
0.32%	0.00446	251.78	4.94
	0.00461	238.54	4.91
	0.00477	237.09	4.26
	0.00501	238.39	4.60
	0.00518	242.18	3.15
	0.00552	222.00	5.83
	0.00611	222.78	4.25
	0.00677	215.24	3.29
	0.00717	214.22	4.92
	0.00725	214.19	3.72
	0.00726	210.84	4.87
	0.00744	202.34	3.68
	0.00764	199.42	3.18
	0.00754	203.68	3.49
	0.00803	201.97	2.82
	0.00839	185.79	3.32
	0.00932	189.63	3.25
	0.01002	187.12	4.42
	0.01010	183.45	2.83
	0.01013	186.70	4.40
	0.01106	176.82	2.90
	0.01166	170.83	2.16
	0.01232	163.44	4.87
	0.01243	160.60	4.84
	0.01253	158.52	3.00
	0.01413	154.45	2.16
	0.01454	151.03	2.60
	0.01498	148.55	2.92
	0.01508	153.71	2.72
	0.01511	146.78	2.90
	0.01728	138.20	2.94
	0.01776	136.77	2.67
	0.01790	135.55	2.65
	0.01911	125.43	2.37
	0.01993	124.29	2.02
	0.02042	123.39	1.76
	0.02212	113.68	2.68
	0.02224	108.04	2.58
	0.02228	109.42	2.62
	0.02453	104.83	1.84
	0.02547	94.89	2.04
	0.02564	97.43	2.08
	0.02806	88.61	1.93
	0.02864	89.77	1.57
	0.02939	85.37	1.37
	0.03203	76.05	1.13
	0.03245	77.96	1.22
	0.03310	78.34	2.03
	0.03329	78.39	2.01
	0.03494	68.30	1.33
	0.03604	67.24	1.01
	0.03897	59.26	1.68
	0.03912	60.27	1.06
	0.03918	61.40	1.72
	0.04215	52.77	0.97
	0.04530	51.35	1.51
	0.04847	44.07	0.95
	0.05552	34.81	0.81
	0.05692	33.38	0.67
	0.06278	26.79	0.67
	0.06455	25.07	0.55
	0.06901	22.39	0.56
	0.07048	21.44	0.53
	0.07236	19.01	0.45
	0.07863	16.04	0.48

	0.00047	1189.59	25.55
	0.00064	659.43	14.99
	0.00100	318.31	6.52
	0.00125	237.35	4.69
	0.00131	219.13	6.10
	0.00133	211.03	3.78
	0.00160	177.24	5.10
	0.00162	164.27	4.85
pp + pp	0.00164	172.79	4.26
	0.00195	138.26	3.27
398 GeV	0.00206	132.95	2.90
	0.00216	133.34	2.75
	0.00225	125.61	2.82
Normalization	0.00227	124.53	2.81
uncertainty	0.00245	121.57	2.76
0.52%	0.00252	116.95	2.41
	0.00283	105.91	2.26
	0.00307	103.98	2.41
	0.00343	100.37	2.85
	0.00346	96.01	2.78
	0.00349	96.61	2.22
	0.00392	93.52	2.39
	0.00414	91.91	1.86
	0.00443	90.80	1.51
	0.00463	87.08	1.74
	0.00474	87.90	1.66
	0.00491	86.13	2.65
	0.00495	82.92	2.60
	0.00527	85.95	1.45
	0.00571	83.91	1.23
	0.00604	83.43	1.69
	0.00646	83.82	1.67
	0.00661	79.44	2.32
	0.00664	83.28	1.50
	0.00665	81.49	2.35
	0.00722	81.04	2.16
	0.00727	81.43	2.17
	0.00752	79.59	1.41
	0.00796	79.01	1.71
	0.00964	73.31	1.40
	0.01008	74.96	1.55
	0.01085	75.38	1.45
	0.01197	71.18	1.30
	0.01246	73.31	1.61
	0.01281	70.31	1.21
	0.01299	74.57	1.61
	0.01455	68.99	1.36
	0.01509	69.20	1.63
	0.01567	70.83	1.42
	0.01602	65.71	1.48
	0.01738	66.30	1.39
	0.01797	66.29	1.45
	0.01838	64.06	1.28
	0.01868	68.03	1.30
	0.01972	66.25	1.29
	0.02047	65.65	1.27
	0.02119	64.04	1.32
	0.02230	60.87	1.29
	0.02391	60.66	1.13
	0.02579	59.26	1.26

	0.00083	623.92	9.80
	0.00108	467.53	10.89
	0.00159	339.93	14.24
	0.00163	335.24	6.16
	0.00188	326.32	10.37
	0.00224	313.28	10.55
	0.00229	295.53	10.45
	0.00254	282.28	4.16
pd + pd	0.00262	294.11	4.47
	0.00290	278.01	4.88
397 GeV	0.00300	269.49	7.26
	0.00305	274.51	11.54
	0.00328	260.60	5.50
Normalization	0.00380	258.14	6.04
uncertainty	0.00431	255.22	6.28
0.36%	0.00437	251.88	6.22
	0.00438	239.75	3.36
	0.00472	239.26	3.15
	0.00485	239.41	2.88
	0.00534	234.34	2.75
	0.00548	238.19	4.44
	0.00633	222.26	2.83
	0.00714	213.64	3.38
	0.00721	212.77	4.58
	0.00792	206.32	5.04
	0.00909	195.55	2.44
	0.00988	195.93	6.87
	0.00996	187.85	4.49
	0.00997	191.70	6.68
	0.01049	180.48	2.35
	0.01237	175.39	4.45
	0.01284	162.43	3.16
	0.01306	165.51	5.25
	0.01398	157.18	2.02
	0.01505	148.92	2.86
	0.01580	147.99	6.34
	0.01592	143.27	6.33
	0.01643	137.99	2.45
	0.01667	139.15	2.73
	0.01783	130.20	2.18
	0.01949	123.30	3.01
	0.02191	118.09	3.42
	0.02203	115.59	2.27
	0.02556	104.03	3.18
	0.02654	95.34	3.37
	0.02670	97.89	3.37
	0.03040	85.24	2.81
	0.03057	84.98	2.76
	0.03127	80.03	1.47
	0.03160	79.56	1.27
	0.03320	75.31	2.68
	0.03546	66.34	1.20
	0.03870	61.62	2.39
	0.03885	57.44	1.22
	0.03888	63.82	2.43
	0.04167	54.07	1.03
	0.04478	47.73	1.85
	0.04495	49.42	1.16
	0.04498	52.43	1.87
	0.05153	41.73	1.74
	0.05175	40.83	1.20
	0.05857	33.85	1.07
	0.05876	33.65	1.10
	0.06602	26.39	1.00
	0.06627	26.10	0.98

TABLE II
Analysis Results

E_{lab} (GeV)	$\rho = \frac{\text{Re } A}{\text{Im } A}$	$\Delta\rho$	$\Delta\rho/\Delta b$ (GeV/c) ²	$\Delta\rho/\Delta\sigma$ (mb) ⁻¹
Reaction pp + pp (Systematic error in ρ_{pp} , ± 0.009)				
52	-0.153	0.012	0.038	-0.033
80	-0.096	0.010	0.036	-0.035
199	-0.034	0.009	0.025	-0.039
261	-0.009	0.009	0.023	-0.032
303	-0.011	0.008	0.024	-0.083
398	+0.012	0.009	0.022	-0.028
Reaction pp + pd (Systematic error in ρ_{pd} , ± 0.008)				
49	-0.110	0.013	0.059	-0.011
82	-0.113	0.010	0.065	-0.011
182	-0.037	0.009	0.058	-0.008
281	-0.031	0.011	0.060	-0.007
379	+0.003	0.010	0.046	-0.007
397	+0.034	0.010	0.057	-0.008

TABLE III

Reaction $p\bar{d} \rightarrow p\bar{d}$

Glauber Analysis Using Eq. (16)

E_{lab} (GeV)	ρ_{pn}	$\Delta\rho_{pn}$	I_G (mb) ⁻¹	ΔI_G (mb) ⁻¹
49	-0.081	0.018	0.0281	0.0011
82	-0.127	0.013	0.0298	0.0006
182	-0.065	0.014	0.0333	0.0005
281	-0.084	0.020	0.0348	0.0006
379	-0.045	0.017	0.0362	0.0005
397	+0.021	0.017	0.0346	0.0007

TABLE IV

Reaction $pd + pd$ Glauber Analysis Using Eq. (19)

E_{lab} (GeV)	ρ_{pn}	$\Delta\rho_{pn}$
82	-0.127	0.021
182	-0.031	0.019
281	-0.052	0.023
379	-0.003	0.021

FIGURE CAPTIONS

Fig. 1: Schematic layout of experiment. The H_2/D_2 gas jet fires vertically (perpendicular to figure). The detectors are on a movable ion guide and at a constant distance of 7.5 m from the beam-jet intersection point.

Fig. 2: Electronics schematic.

Fig. 3: Typical deuteron elastic peak vs. momentum distribution.

Fig. 4: Proton-proton differential cross section at beam energy 398 GeV. Fitted parameters: Normalization $0.3593 \pm 0.0019 \frac{mb}{(GeV/c)^2}$, $\rho = 0.0121 \pm 0.0085$, $\chi^2/N_{pts} = 76/61$.

Fig. 5: Proton-deuteron differential cross section at beam energy 379 GeV. Fitted parameters: Normalization $0.2647 \pm 0.0008 \frac{mb}{(GeV/c)^2}$, $\rho = 0.003 \pm 0.010$, $\chi^2/N_{pts} = 96/79$.


Fig. 6: The ratio of the real to the imaginary part of the forward p-p nuclear amplitude. The curves are I (dashed) one Pomeron formula $ReA = \frac{\pi}{2} \frac{\partial}{\partial \ln S} \frac{Im A}{S}$, II (solid) a dispersion relation calculation discussed in text. o - Ref. 17
 - Ref. 5. X - Present experiment.

Fig. 7: The ratio of the real to the imaginary part of the forward p-d nuclear amplitude. The solid line is the best fit $\rho(s) = -0.450 + 0.070 \ln S_{pp}$ to the proton-deuteron results. The dashed line is our fit $\rho(s) = -0.490 + 0.076 \ln S_{pp}$ to the proton-proton results. o - Ref. 6. X - Present experiment.

Fig. 8: The ratio of the real to imaginary part of the forward

p-n amplitude. The error corridor shown is from the empirical fit $\rho(s) = (-0.490 \pm 0.034) + (0.076 \pm 0.006) \ln S_{pp}$ to the proton-proton results. o - Ref. 8.
x - Present experiment.

Fig. 9: The Glauber integral, I_G , as a function of energy.

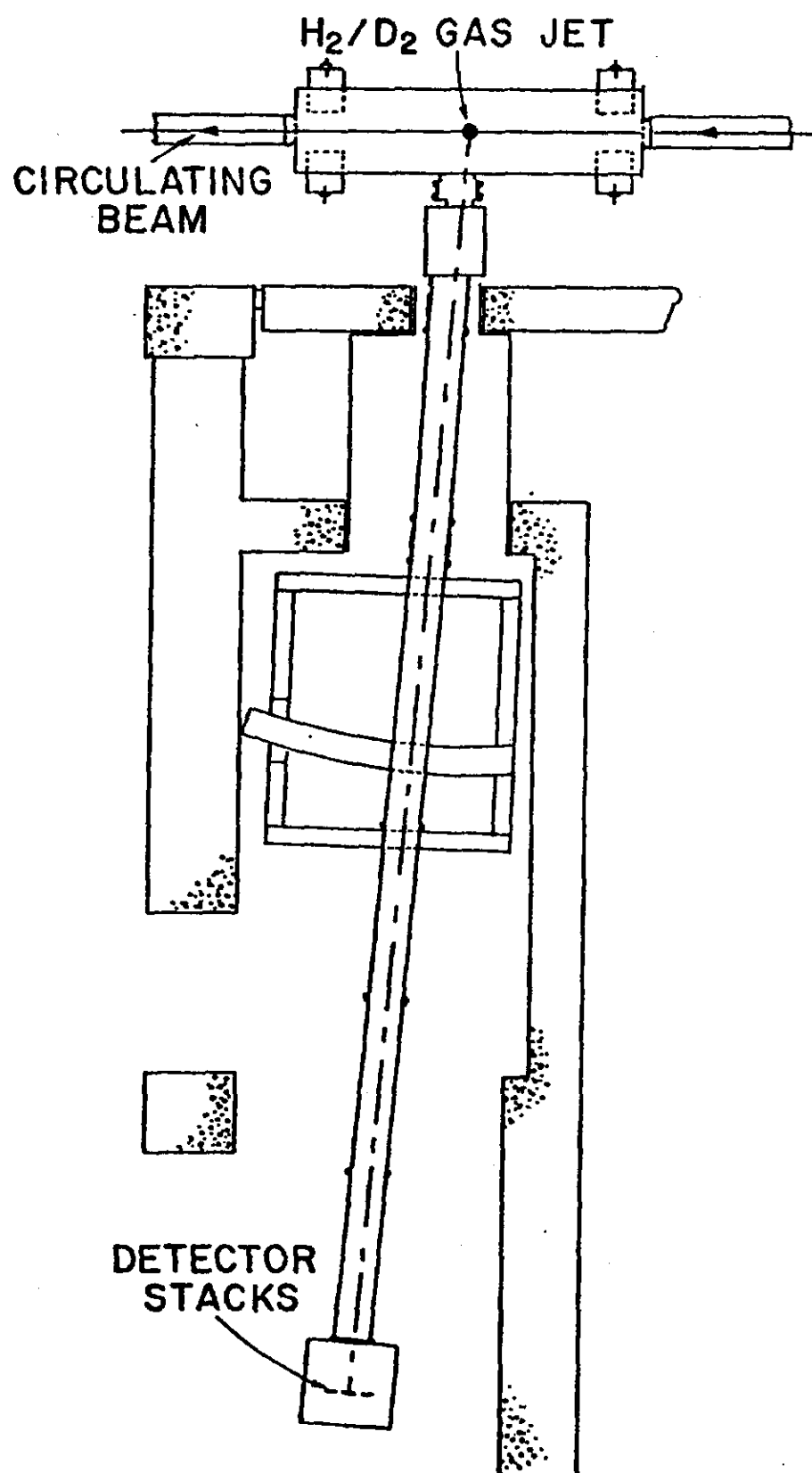


Figure 1

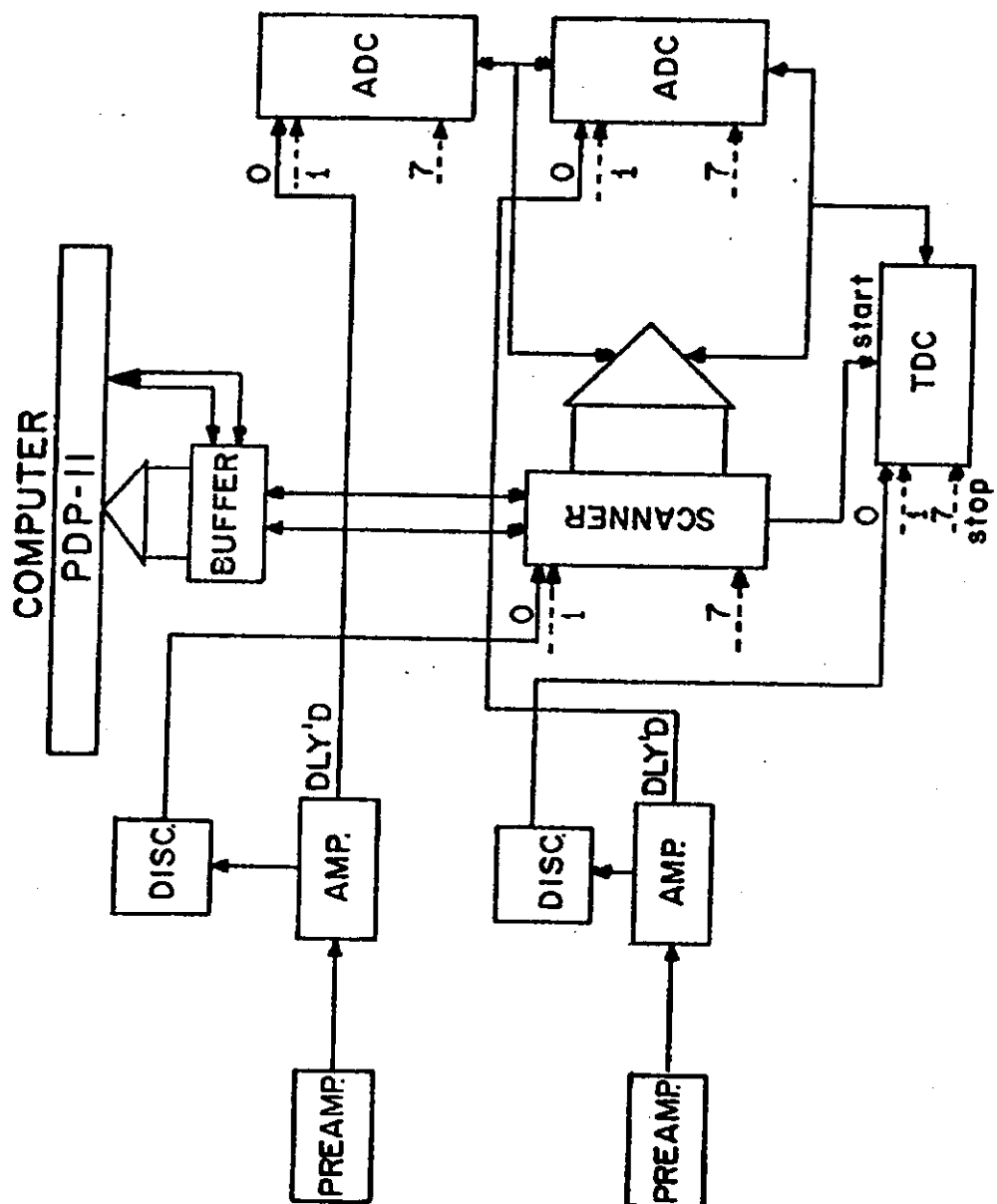


Figure 2

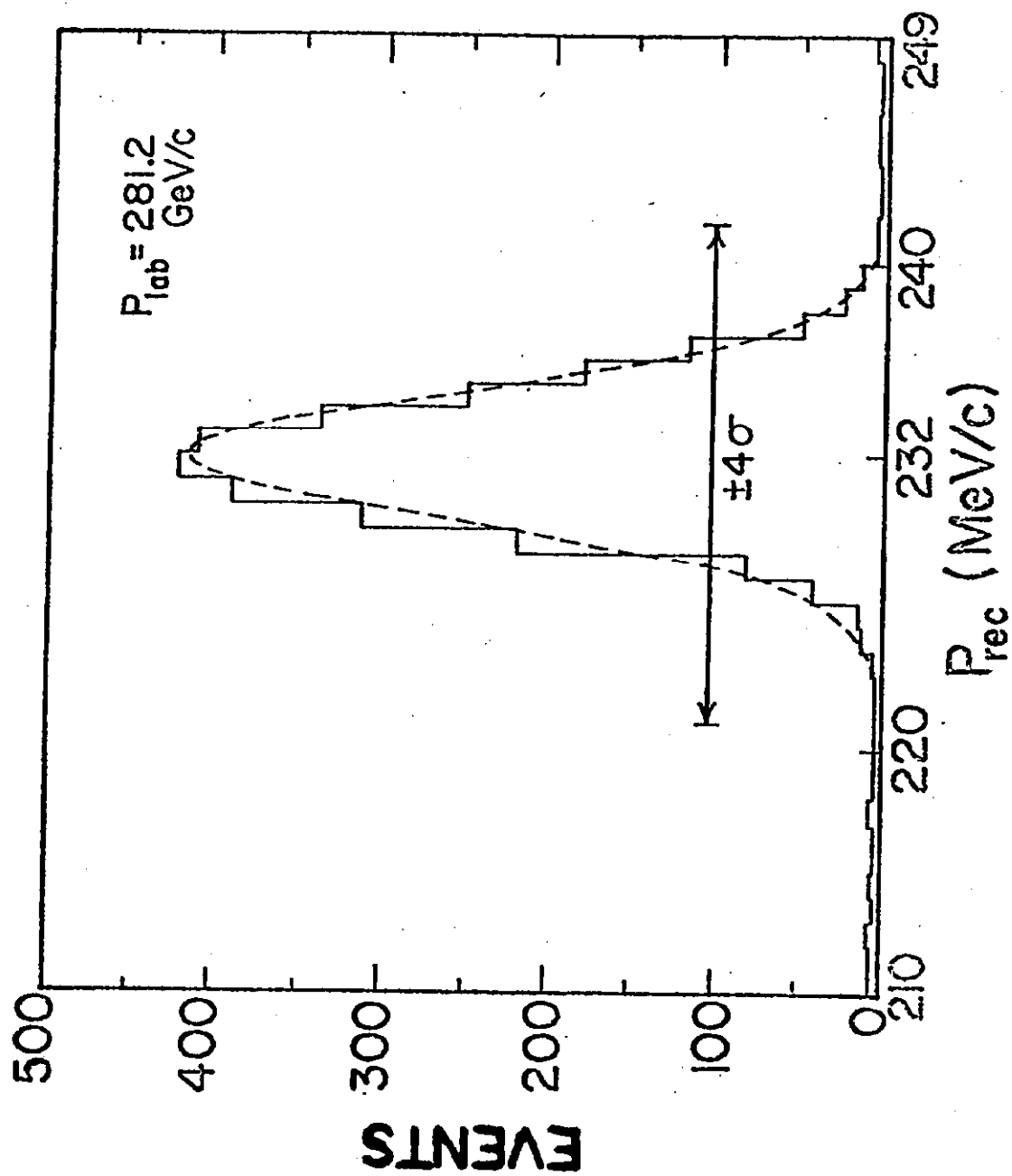


FIGURE 3

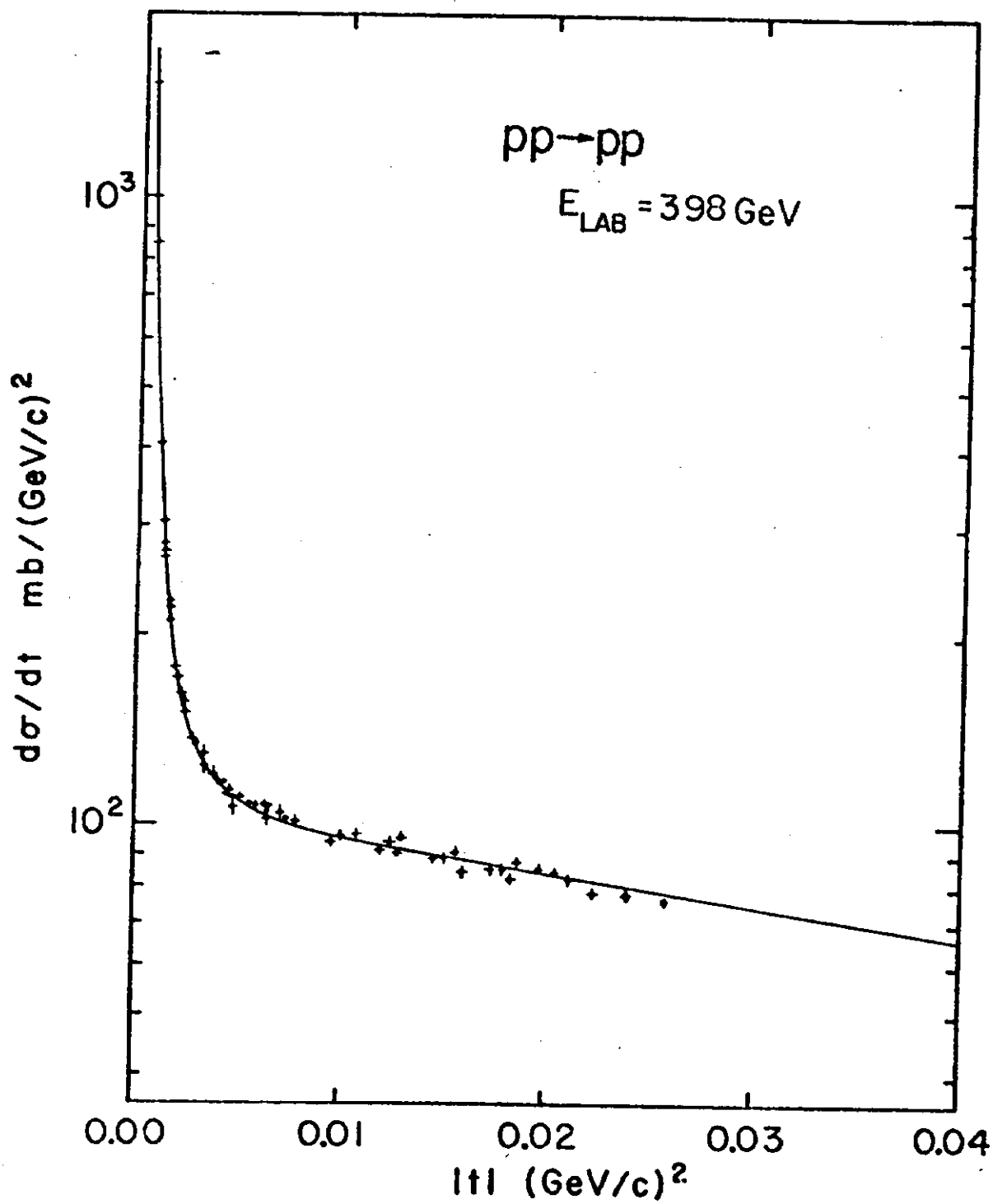


Figure 4

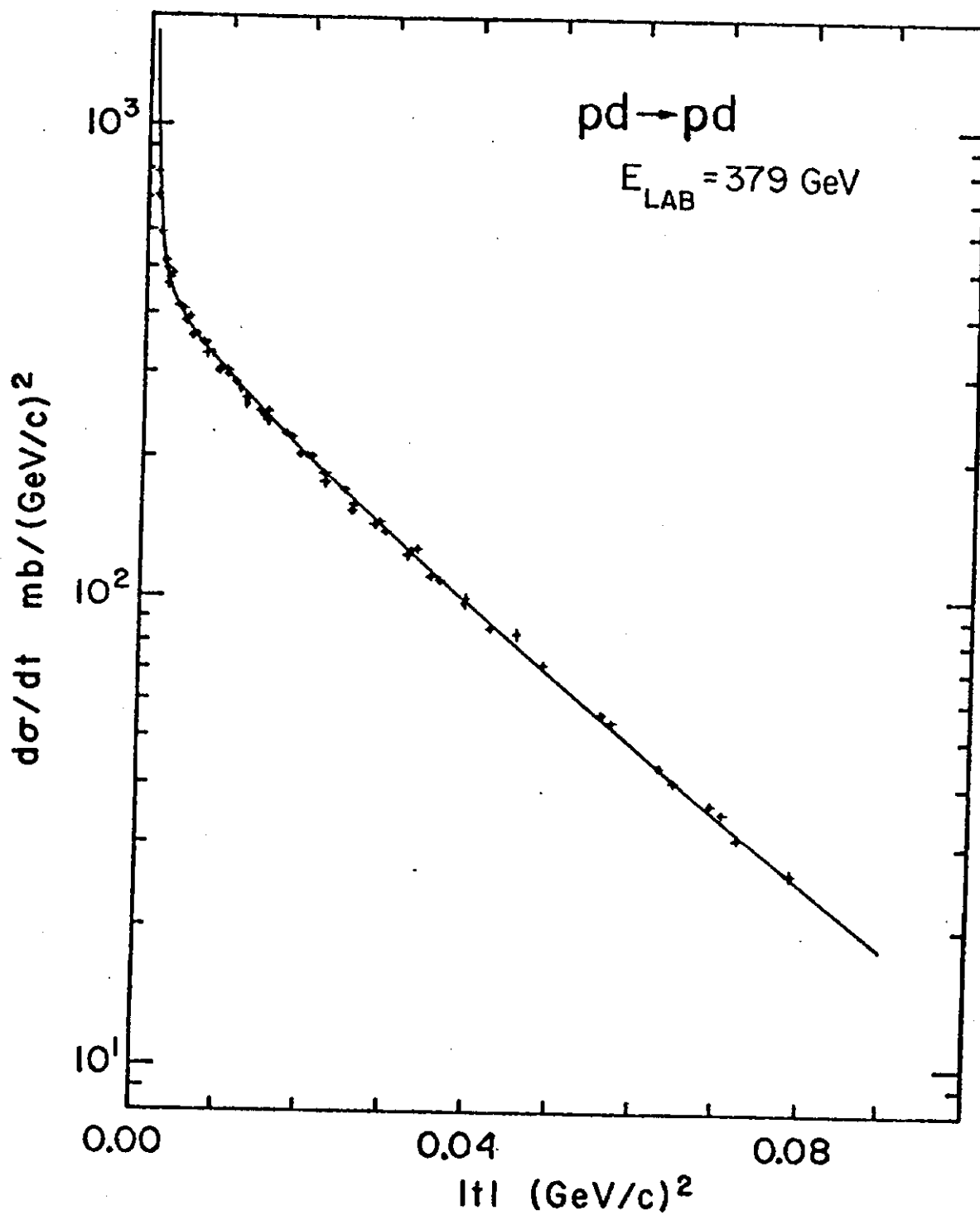


Figure 5

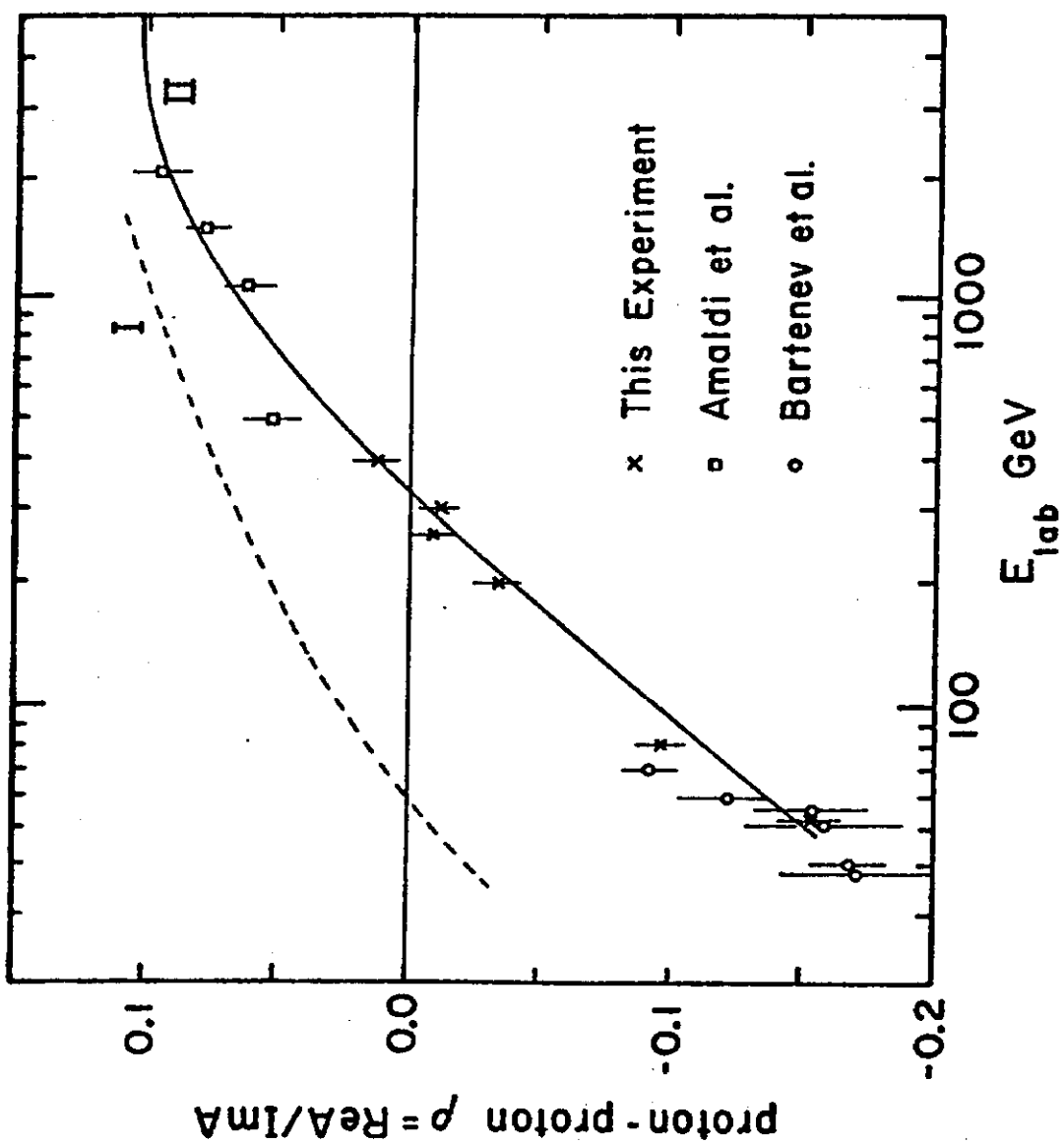


Figure 6

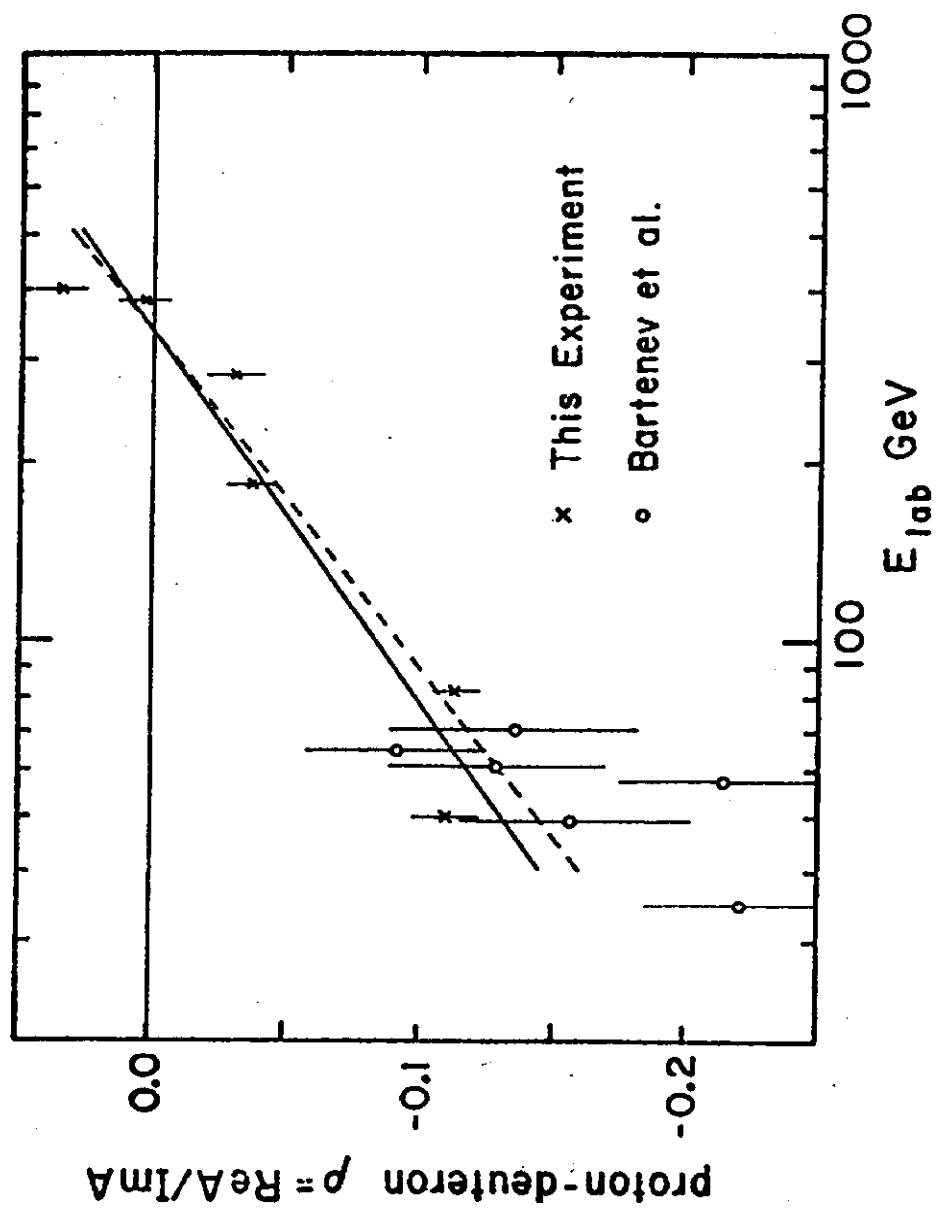


Figure 7

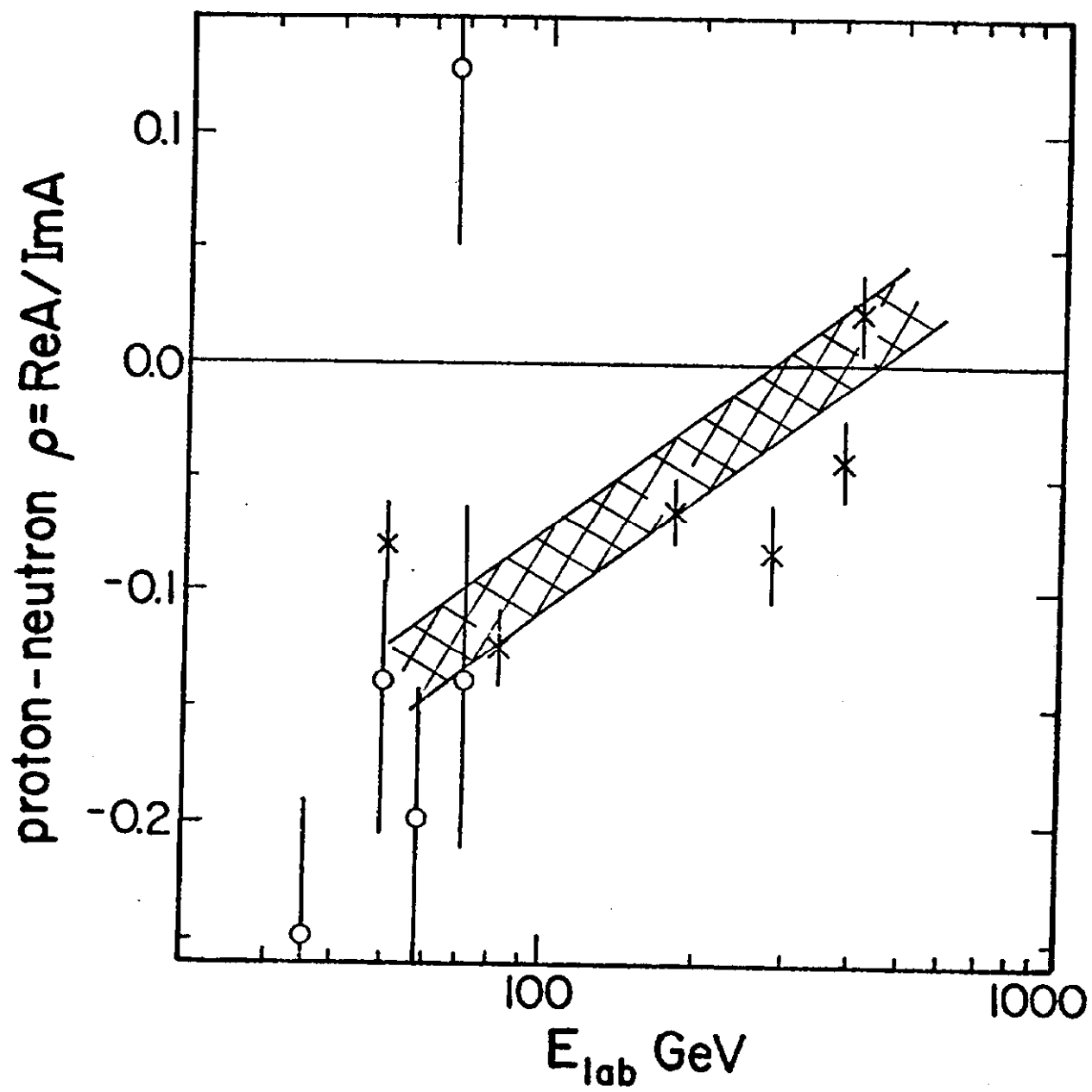


FIGURE 8

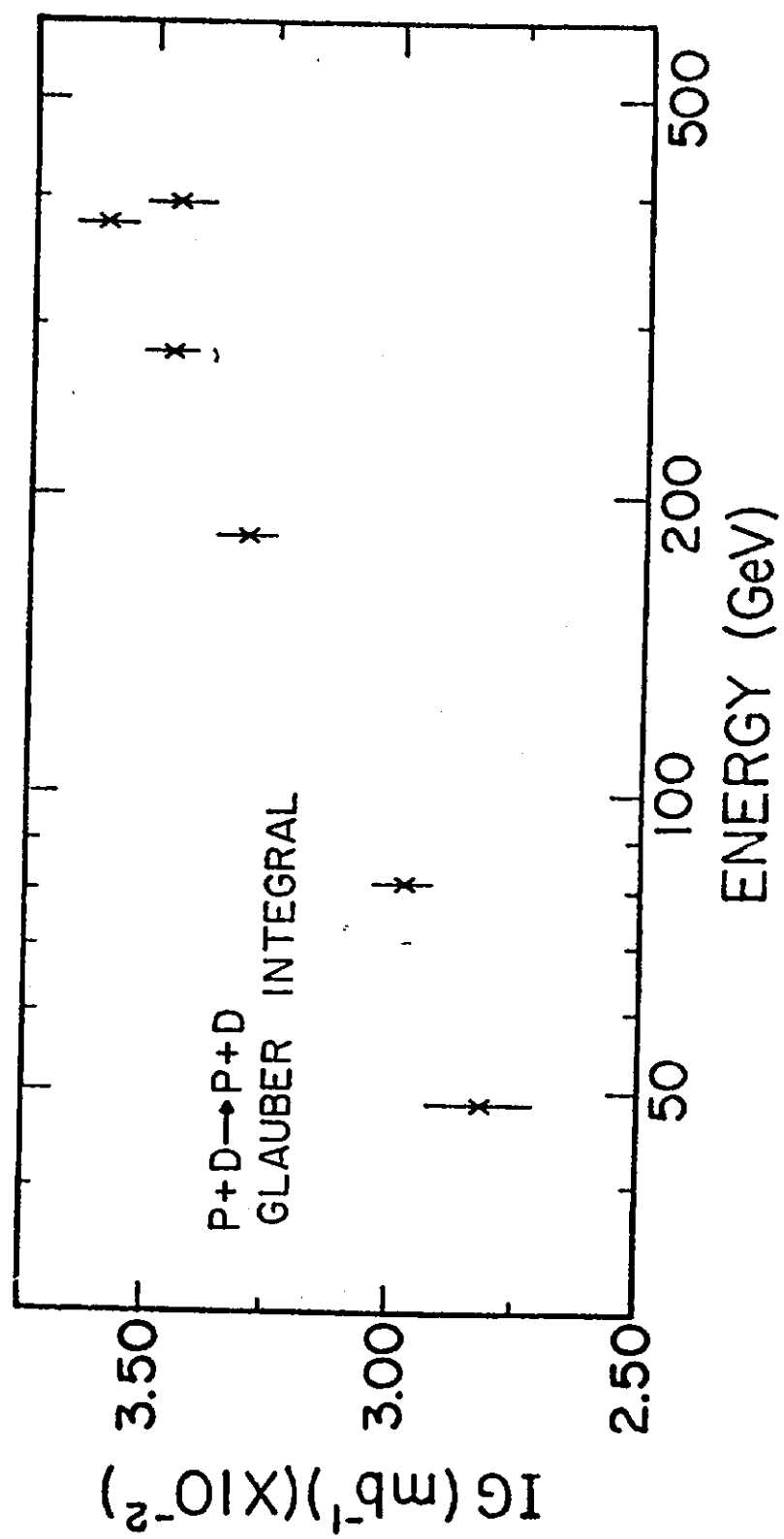


FIGURE 9